IEEE Access
Multidisciplinary | Rapid Review | Open Access Journal

Received February 19, 2021, accepted March 16, 2021, date of publication March 30, 2021, date of current version April 12, 2021.

*Digital Object Identifier 10.1109/ACCESS.2021.3069870*

# Generalized Design Technique of Ultra-Wideband Transitions for Quasi-TEM Planar Transmission Lines Based on Analytical Models

**GWAN HUI LEE[1], (Student Member, IEEE), SACHIN KUMAR[1], WAHAB MOHYUDDIN[2], (Member, IEEE), HYUN CHUL CHOI[1], AND KANG WOOK KIM[1], (Member, IEEE)**

[1]School of Electronic and Electrical Engineering, Kyungpook National University, Daegu 41566, South Korea
[2]Research Institute for Microwave and Millimeter-Wave Studies, National University of Sciences and Technology, Islamabad 44000, Pakistan

Corresponding author: Kang Wook Kim (kang_kim@ee.knu.ac.kr)

This work was supported in part by the National Research and Development Program through the National Research Foundation of Korea (NRF) funded by the Ministry of Education, Science and Technology, under Grant NRF-2019M1A7A1A02085630, and in part by the BK21 FOUR project funded by the Ministry of Education, Korea (4199990113966).

**ABSTRACT** A generalized design technique of ultra-wideband planar transitions using EM-based analytical models is presented in this paper. Among various planar transmission lines, each transmission line has unique advantages over other line types, and a microwave component in a system can be designed to perform much better if it is implemented on a certain type of transmission line. Therefore, low-loss and high-performance transitions between transmission lines, with easy integrability with the main circuit board, are needed. The proposed transition design technique uses the Schwarz-Christoffel transformation, which is one of conformal mapping methods, and can be applied to design any planar transition between a pair combination of planar transmission lines based on TEM or quasi-TEM waves. To optimally match the characteristic line impedance and smoothly transform the electromagnetic field distribution between the planar transmission lines, entire cross-sections through the planar transition should be analyzed with proper models. In this paper, the cross-sections of planar transitions are categorized into 4 cross-sectional models, where each cross-section is divided into multiple regions for the analysis to obtain line capacitance. Therefore, for the 4 cross-sectional models, 7 types of basis structures are identified to obtain their capacitances by applying conformal mapping. By adding capacitances of a combination of the 7 analysis types, the total line capacitance, thus the characteristic line impedance, of any cross-sectional model of the planar transition can be obtained. The characteristic line impedance of each cross-sectional model calculated with the proposed analytical formulas is compared with the 3D EM calculations, and it is found that the deviated values are mostly well under 6%. This proposed technique enables to design various planar transitions efficiently and quickly for the maximum performance without parameter tuning trials, by providing optimal impedance matching and smooth field transformation up to mm-wave frequencies.

**INDEX TERMS** Conformal mapping, cross-sectional model, planar transition, planar transmission line, Schwarz-Christoffel transformation.

## I. INTRODUCTION

In order to support ever-increasing high-speed digital data transmission for the 5$^{th}$ (and beyond 5$^{th}$) generation mobile communications, microwave and mm-wave components with high performance and wide frequency bandwidth will become more important. Transceivers with microwave and mm-wave components can transmit data at multi-Gb/s by using wide bandwidth monolithic microwave integrated circuits (MMICs) and high-performance wide-band packaging [1]–[10]. Digital data, consisting of rectangular data shapes with sharp rise-/fall-edges, occupies huge frequency bandwidth as the digital data speed increases. Therefore, the signal transmission lines with their curves or bends,

The associate editor coordinating the review of this manuscript and approving it for publication was Fulvio Schettino.

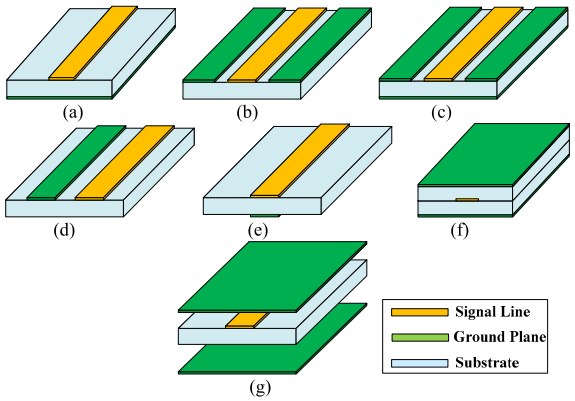


**FIGURE 1.** Planar transmission lines: (a) microstrip line (MSL), (b) coplanar waveguide (CPW), (c) conductor-backed coplanar waveguide (CBCPW), (d) coplanar strip (CPS), (e) parallel strip line (PSL), (f) strip line (SL), (g) suspended strip line (SSL).

split/combining joints, and via connection to different layers should provide very wide bandwidth in order to preserve the signal integrity for the fast-speed digital data. Unless the signal lines in a multi-layered substrate are carefully designed, as the operating frequency increases, multiple undesirable phenomena such as spurious EM coupling, resonances, and impedance mismatching may occur, causing serious distortion of signal shapes as well as spurious EM interference by the leaked signals.

Most of microwave and mm-wave components in a communication system module are implemented using microstrip lines, but various microwave components can perform better if other planar transmission lines are utilized. The configurations of planar transmission lines such as microstrip line (MSL), coplanar waveguide (CPW), conductor-backed coplanar waveguide (CBCPW), coplanar strip (CPS), parallel stripline (PSL), stripline (SL), and suspended stripline (SSL), are shown in Fig. 1. Here, a transition is a structure which connects between two transmission lines. Therefore, if there exist high-performance transitions, some microwave/mm-wave components can be designed to have much better performance by taking advantages of a certain transmission line. For example, various transitions for transmission lines were used for filters, couplers, dividers, and amplifiers [11]–[20]. Also, a balun designed in a form of a transition was used to feed the antenna system [21], [22].

Each planar transmission line has unique advantages and short-comings as compared with other line types [23]–[30]. Also, the configuration of the physical structure including the signal line and ground line(s) (or ground plane(s)) of a certain planar transmission line is different from those of other lines (Fig. 1). Most of the planar transmission lines possess some parasitic modes due to discontinuity at the substrate-air interface, thus exhibiting the quasi-transverse electromagnetic (TEM) mode. The properties of various TEM/quasi-TEM mode-based planar transmission lines in terms of structure, polarity balance type, transmitting mode, radiation, Q-factor, and characteristic line impedance, are listed in Table 1. CPW and CPS are one-sided structures, but the other planar transmission lines are double-sided structures. A balanced line (CPS or PSL) can be used as an input line for balanced circuits, e.g., a feed line for balanced antennas. SL and SSL are used in circuit applications requiring high Q-factor, e.g., filter designs with high selectivity. Each planar transmission line has a different range of the characteristic line impedance. In Table 1, the range of the characteristic line impedance is calculated using a substrate with dielectric constant of 2.2 and thickness of 10 mil by considering the typical PCB fabrication limits. For example, a CPS is a balanced line with impedance range of about 100 $\sim$ 200 $\Omega$, while an MSL is an unbalanced line with impedance range of about 25 $\sim$ 130 $\Omega$ within typical fabrication limits. Also, the electric field line shapes of one transmission line are different from those of another.

A transition is a connecting structure between two transmission lines. Sometimes, the target transmission lines may have the same characteristic line impedance, and, in this case for the maximum wideband performance, the line impedance through the transition structure can be maintained at the same line impedance value. In many cases, however, different characteristic line impedances are required for the target transmission lines. In those cases, to design a high-performing wideband transition structure, an optimal impedance matching between the transmission lines, e.g., in the form of an impedance taper or a multi-section impedance transformer, can be applied.

A planar transition structure connecting two planar transmission lines can consist of signal line(s), ground line(s), dielectric substrate(s), and via(s). Depending on the shape and location of these constituting elements (i.e., transition design parameters), the characteristic line impedance of the transition can be determined. Therefore, by adjusting the transition design parameters, an optimal impedance matching from a planar transmission line to the other line can be achieved. To obtain the required line impedances for every locations of the planar transition, the design parameters can be adjusted using a parameter-tuning process with an EM simulator, which can be quite time-consuming. However, if the analytical formulas of the line impedance for any cross-sectional area of the transition with various dielectric substrates can be obtained, the transition design process can be very fast and efficient. Another important design consideration is that, for the optimized wideband transition performance, the planar transition structure should provide smooth transformation of the electric field line shape of one planar transmission line onto that of the other transmission line.

Until now, various designs of the planar transitions have been reported, and most of the planar transitions are designed from an MSL to other planar transmission lines. In [31], [32], CPS-to-MSL transitions with a radial stub and modified ground plane were designed. Here, the radial stub was used as a resonant stub at the end of the CPS ground line. In [31], a long CPS-to-MSL transition was designed to have operating bandwidth from 1.3 GHz to 13.3 GHz in the presence

**TABLE 1. Properties of planar transmission lines.**

| Transmission Line | Structure | Type | Mode | Radiation | Q-factor | Characteristic Line Impedance* |
|---|---|---|---|---|---|---|
| MSL | Double-sided | Unbalanced | Quasi-TEM | Low | Low | 24~128 Ω |
| CPW | One-sided | Unbalanced | Quasi-TEM | Medium | Low | 59~132 Ω |
| CBCPW | Double-sided | Unbalanced | Quasi-TEM | Low | Low | 23~110 Ω |
| CPS | One-sided | Balanced | Quasi-TEM | High | Low | 110~203 Ω |
| PSL | Double-sided | Balanced | Quasi-TEM | High | Low | 27~228 Ω |
| SL | Double-sided | Unbalanced | TEM | Low | High | 16~94 Ω |
| SSL | Double-sided | Unbalanced | Quasi-TEM | Low | High | 97~235 Ω |

*Dielectric constant of the substrate: 2.2, height of the substrate: 10 mil, height of the strip line: 20 mil, gap between two conductors: 5 mil, linewidth range: 4~80 mil.

of a high impedance difference between the CPS (185 Ω) and MSL (50 Ω). In [32], a short CPS-to-MSL transition was designed with the operating bandwidth of 5.1 GHz to 6.1 GHz.

In [33], [34], the MSL-to-CPW and PSL-to-CPW transitions were reported with bandwidths of 2.8 GHz to 7.5 GHz and 1.9 GHz to 9 GHz, respectively. The operating bandwidth was limited due to a large signal linewidth change by the radial stubs. A CPS-to-PSL transition was reported with a frequency range from 2.4 GHz to 10.7 GHz [35]. In this transition, the radial stubs were connected to a CPS ground line. Also, due to the high impedance difference between the CPS (148 Ω) and PSL (50 Ω), a long transition length was used. A CBCPW-to-SL transition was reported to have a wide frequency range from 6 GHz to 28.4 GHz, where the 50 Ω line impedance was maintained throughout the transition [36]. Here, the signal lines of the CBCPW and SL were connected by a via with a circular aperture under the substrate. In [37], a PSL-to-MSL transition with a wideband performance from 1 GHz to 30 GHz was reported, maintaining at 50 Ω line impedance through the transition. For the smooth electric field transformation, the ground plane was reduced by forming an arc line. Most of the reported planar transitions, however, were designed by the parameter variation trials without a systematic design guideline. If the design conditions change, the parameter tuning process should be performed again.

On the other hand, various designs of high-performing planar transitions were proposed by the authors' group using the Schwarz-Christoffel transformation, which is one of conformal mapping methods, to obtain the characteristic line impedance of each cross-sectional area of the transition in analytical formulas [38]–[42]. A CPW-to-MSL transition was designed with a frequency range from 7 GHz to 40 GHz, maintaining the impedance at 50 Ω [38]. A PSL-to-CPW transition was designed from 40 MHz to 27 GHz with maintaining the impedance at 50 Ω [39]. An SSL-to-MSL transition was designed from 40 MHz to 30 GHz [40]. In [41], an asymmetric CPS-to-MSL transition was designed, where the line impedance was tapered from a 147 Ω coplanar strip line to a 50 Ω microstrip line. This transition showed ultra-wideband performance from 6 GHz to 40 GHz. A CPS-to-PSL transition was designed with ultra-wideband performance (6.4 GHz to 40 GHz), where the line impedance was tapered from a 147 Ω CPS to a 50 Ω PSL [42]. In Table 2, the characteristics and performance of the reported transitions are compared.

**TABLE 2. Comparison of the reported planar transitions.**

| Ref. | Structure | Characteristic Line Impedance [Ω] | Operating Bandwidth [GHz] | Analytical Model |
|---|---|---|---|---|
| [31] | CPS-MSL | 185/50 | 1.3-13.3 | X |
| [32] | CPS-MSL | 88/50 | 5.1-6.1 | X |
| [33] | MSL-CPW | 50/50 | 2.8-7.5 | X |
| [34] | PSL-CPW | 50/50 | 1.3-9 | X |
| [35] | CPS-PSL | 148/50 | 2.4-10.7 | X |
| [36] | CBCPW-SL | 50/50 | 6-28.4 | X |
| [37] | PSL-MSL | 50/50 | 1.0-30.0 | X |
| [38] | CPW-MSL | 100/50 | 7-40 | O |
| [39] | PSL-CPW | 50/50 | 0-27 | O |
| [40] | MSL-SSL | 50/50 | 0-30 | O |
| [41] | MSL-CPS | 147/50 | 6-40 | O |
| [42] | CPS-PSL | 147/50 | 6.4-40 | O |

* X: transition design without an analytical model. O: transition design with an analytical model.

In this paper, a generalized design procedure of ultra-wideband planar transitions for any pair combination of planar transmission lines is proposed. This transition design method is a traveling-wave type with optimal impedance matching and smooth field transformation (TW-IMFT). The cross-sectional area of the transition is analyzed to obtain characteristic line impedance using the Schwarz-Christoffel transformation. Among various planar transition configurations between any pair of the planar transmission lines, four cross-sectional models (Section II(A)) have been identified. Also, in order to systematically analyze the cross-sectional models, seven analysis types (Section II(B)) have been defined. Any cross-sectional model consists of a combination of the seven analysis types, which have analytic solutions (Section II(C)). The proposed design technique can be applied to the wideband TW-IMFT-type transitions, but may not be applied to the resonant-type transitions with relatively narrow-bandwidth. The proposed analysis is assuming the TEM/quasi-TEM mode propagation, and the conductor thickness is assumed to be very thin. Fringe field effects

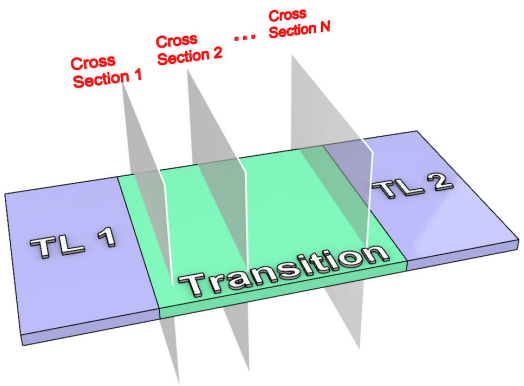


**FIGURE 2.** Perspective image of a planar transition connecting two planar transmission lines with transitional cross-sections (TL: transmission line).

are accounted in the analysis model. The obtained analytical formulas for the characteristic line impedance are accurate with good approximations, and the validity of the proposed analysis models is discussed with comparison of full 3D EM simulation results.

## II. ANALYTICAL DESIGN TECHNIQUE OF PLANAR TRANSITIONS

A perspective image of a planar transition between two planar transmission lines with several transitional cross-sections is depicted in Fig. 2. Each planar transmission line may have a different range of characteristic line impedance as shown in Table 1, and, therefore, the transition should provide impedance matching between the two lines for the maximum performance. Also, the shapes of electric field lines supported by the two lines may be different, and the transition should adequately conform the field lines.

### A. CROSS-SECTIONAL MODELS OF PLANAR TRANSITIONS

In order to systematically analyze the characteristic line impedance of the cross-sectional area of a planar transition connecting any pair of planar transmissions (listed in Table 1), four cross-sectional models are identified as illustrated in Figs. 3 (a) to (d). The cross-sectional models consist of the signal line (yellow color), ground line/plane (green color), ground wall (green color), and a dielectric substrate (blue color). The widths of the signal line(s) and ground line(s) (or ground plane(s)) can be adjusted to attain a proper characteristic line impedance for impedance matching and to smoothly transform electric fields to conform the field shapes of the two lines.

In Fig. 3(a), an asymmetric CBCPW line with a ground aperture (Model I) is illustrated. In Model I, the characteristic line impedance as well as the electric field line shape can be changed by varying the signal linewidth, the gaps of CBCPW, and the ground aperture. Fig. 3(b) shows a CPS line with an asymmetric ground plane (Model II). The top and the bottom ground lines are connected by a ground wall (using an array of vias). The desired characteristic line impedance can be obtained by modifying the linewidths and gap width of the CPS line with the bottom ground plane. Also, Fig. 3(c)

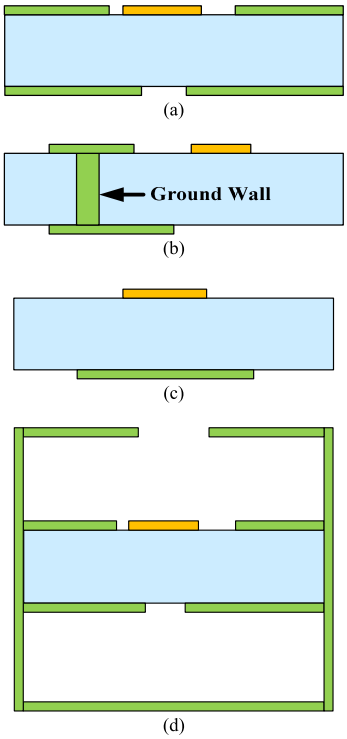


**FIGURE 3.** Cross-sectional models of the planar transition: (a) Model I: CBCPW with a ground aperture, (b) Model II: CPS with an asymmetric ground plane, (c) Model III: asymmetric PSL, (d) Model IV: CBCPW with a ground aperture and shield plates.

illustrates an asymmetric PSL (Model III). The characteristic line impedance can be adjusted by varying the linewidths of the signal line and ground plane. Finally, Fig. 3(d) illustrates an asymmetric CBCPW line with a ground aperture (Model I) enclosed by top and bottom shield plates (Model IV). In Model IV, the top shield aperture and the top and bottom shield plates spacing can be additionally adjusted to obtain the desired characteristic line impedance and field shape.

The Model IV can be used for a planar transition from an SSL to other transmission lines such as MSL, CPW, CPS, PSL, etc. At the SSL side, a top shield plate with a closed slot should be used. On the other hand, other planar transmission lines may not need the top and bottom shield plates. Since the top slot also affects the characteristic line impedance, the transitional line impedance can be adjusted by widening the top slot width together with other design parameters to adequately match another transmission line at the other end of the transition. The effect of the bottom shield plate can be decreased by reducing the bottom aperture width.

A planar transition structure connecting any pair of planar transmission lines can be constructed by a combination of the four cross-sectional models. Four design examples of ultra-wideband planar transitions developed by the authors' group can be described by the proposed cross-sectional models (Model I-IV). Firstly, as shown in Fig. 4, an MSL-to-CPW transition [43] can be formed just by using Model I. The section from *BB'* to *CC'*, which is a symmetric case of the Model I, is the MSL-to-CPW transition. In the design,

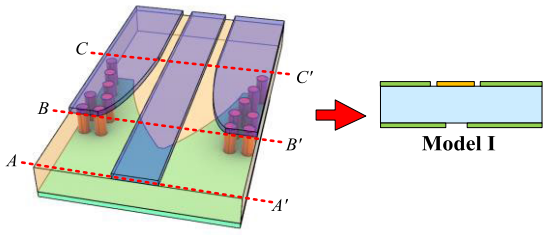


**FIGURE 4.** MSL-to-CPW transition.

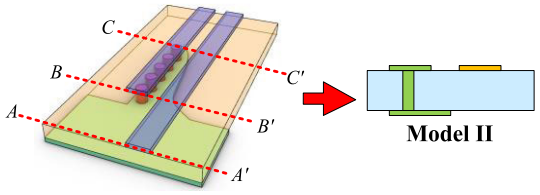


**FIGURE 5.** MSL-to-CPS transition.

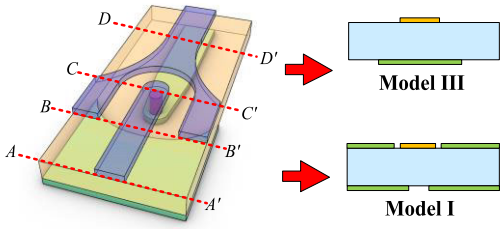


**FIGURE 6.** MSL-to-PSL transition.

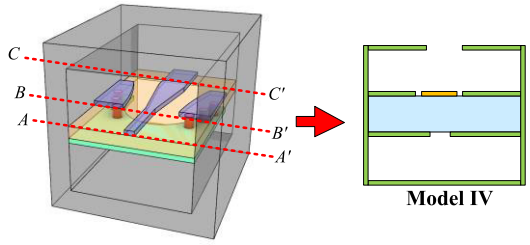


**FIGURE 7.** MSL-to-SSL transition.

the characteristic line impedance of 50 Ω was maintained throughout this transition from the MSL to CPW to have the maximum frequency bandwidth. As a second example, Fig. 5 illustrates an MSL-to-CPS transition [41], and this transition can be designed by using Model II. In this design, the microstrip impedance was 50 Ω, and the CPS impedance was 147 Ω, thus requiring the optimal impedance tapering through the transitional structure. The section from *BB'* to *CC'* is the transitional structure (Model II), and the characteristic line impedance value could be adjusted by changing the width of the via-connected ground line.

As the third example, an MSL-to-PSL transition with phase inversion [42] can be designed using the Model I (*BB'* to *CC'*) and Model III (*CC'* to *DD'*) as shown in Fig. 6. In the design, the phase inversion took place at *CC'*, and the characteristic line impedance was maintained at 50 Ω. As the last example, an MSL-to-SSL transition in Fig. 7 [40] can be formed by using Model IV. The section from *BB'* to *CC'*

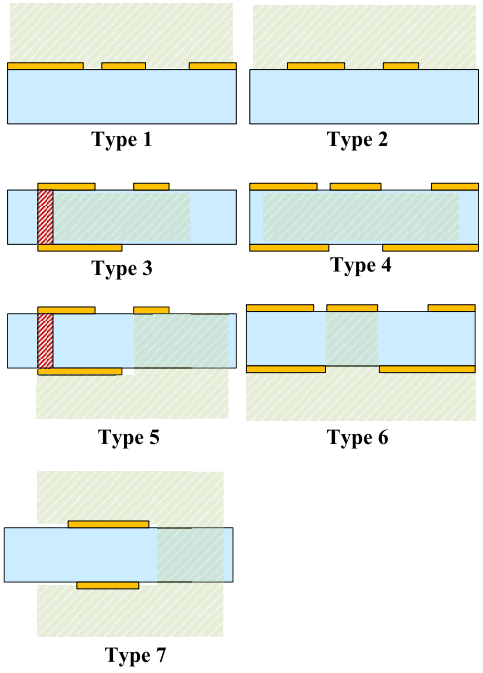


**FIGURE 8.** Seven types of analysis configurations.

is the transitional section. In this design, the characteristic line impedance was also maintained at 50 Ω throughout the transition.

The reported transitions in [38]–[42] showed ultra-wideband performance, and their designs were verified by comparing the measured results with 3D EM simulations. However, those transition design methods were not extended to propose a general and systematic design approach. It should also be noted that there can be many different configurations for a specific planar transition even using this proposed design method. Therefore, in a similar way to the above design examples, any planar transition connecting a pair of planar transmission lines can be implemented as a combination of the proposed four cross-sectional models.

### *B. CALCULATION OF LINE CAPACITANCE*

Each cross-sectional model of a planar transition is divided into multiple analysis regions (typically 3∼4 regions) so that the conformal mapping (Schwarz-Christoffel transformation) can be applied to determine characteristic line impedance. These analysis regions out of the four cross-sectional models are categorized into seven types of analysis configurations as shown in Fig. 8. Each analysis type consists of the conductor (yellow color), substrate (blue color), ground wall (red color), and analysis region (striped green color). The copper line or plane is laminated on the top and bottom layers of the substrate with thin thickness. The ground wall inside the substrate is implemented by an array of vias, and it is assumed to be a simple rectangular wall for the analysis. Since the analysis region becomes a polygon shape, the Schwarz-Christoffel transformation of conformal mapping (based on the TEM

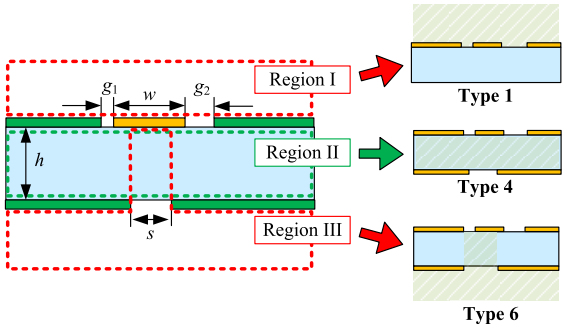


**FIGURE 9.** Model I with analysis regions.

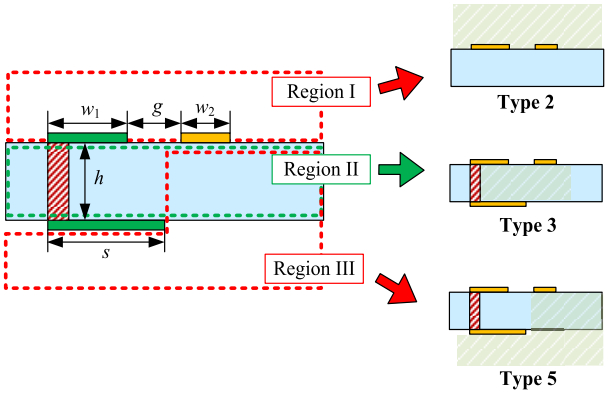


**FIGURE 10.** Model II with analysis regions.

wave analysis) can be applied to map a transition structure into a parallel plate.

The characteristic line impedance of each cross-sectional model can be evaluated by a sum of line capacitances of the analysis types constituting the cross-sectional model. Model I is an asymmetric CBCPW with a ground aperture as shown in Fig. 9, where the analysis regions of the Model I consist of Type 1, Type 4, and Type 6. Also, Model II is an asymmetric CPS with a finite bottom ground plane as shown in Fig. 10, where the analysis regions of the Model II are composed of Type 2, Type 3, and Type 5.

On the other hand, Model III is an asymmetric PSL transition as shown in Fig. 11, where Region I and Region III are the analysis regions located at the right-side and left-side of the conductor line. Region II is a parallel plate area, located at the center of the conductor plane. Finally, Model IV is similar to Model I with top and bottom conductor shield plates and a top shield-plate aperture as shown in Fig. 12. In this model, the Region I and Region II can be analyzed by Type 4, and the Region III can be analyzed by Type 6.

*Type 1:* Type 1 is the analysis region for the upper half-plane (in the air) of an asymmetric CPW as shown in Fig. 13(a). In this analysis, due to the infinite ground linewidth, the signal linewidth $w$ with gaps $g_1$ and $g_2$ are only considered for calculating line capacitance in the $z$-plane. The parameters in the $z$-plane with the mapping angles are listed in Table 3.

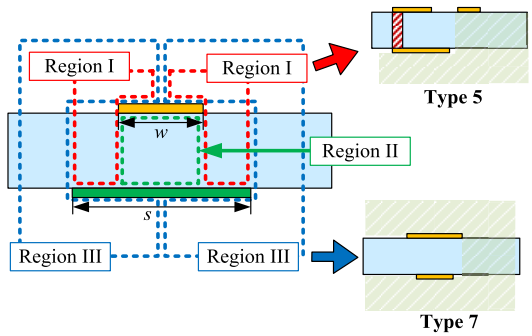


**FIGURE 11.** Model III with analysis regions.

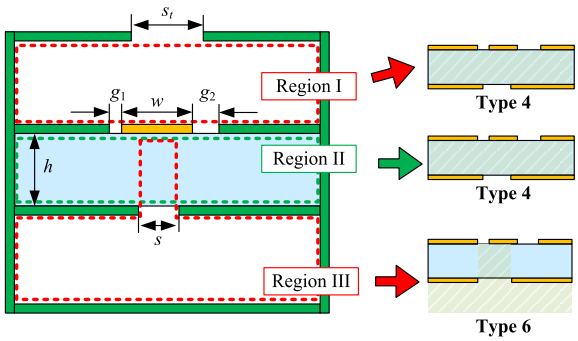


**FIGURE 12.** The Model IV with analysis regions.

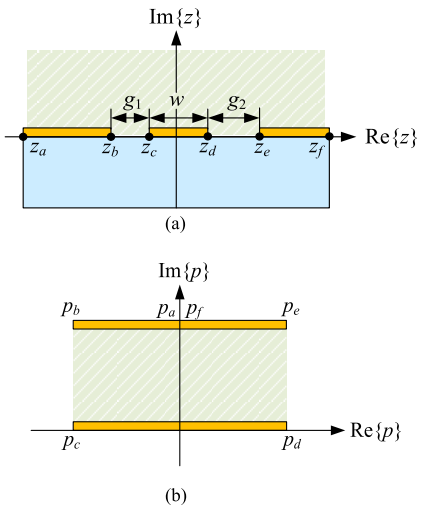


**FIGURE 13.** Schwarz-Christoffel transformation for the conventional CPW (Type 1): (a) $z$-plane, (b) $p$ -plane.

With the 90° mapping points at $z_b$, $z_c$, $z_d$, and $z_e$ in the $z$-plane, the asymmetric CPW can be mapped into a parallel plate in the $p$-plane as shown in Fig. 13(b), using the Schwarz-Christoffel transformation [44]. By considering the parallel plate region in the $p$-plane, the line capacitance $C_1$ of Type 1 is calculated in the form of the elliptical integral of the first kind $K$ as

$$C_1 = \varepsilon_0 \left| \frac{p_e - p_b}{p_e - p_d} \right| = \varepsilon_0 \frac{K(k_1)}{K(k_1')} \tag{1}$$

**TABLE 3.** Parameters of Type 1 in the z-plane.

| Parameter | $z$-plane | Mapping angle |
|---|---|---|
| $z_a$ | $-\infty$ | n/a |
| $z_b$ | $-g_1-w/2$ | $\pi/2$ |
| $z_c$ | $-w/2$ | $\pi/2$ |
| $z_d$ | $w/2$ | $\pi/2$ |
| $z_e$ | $g_2+w/2$ | $\pi/2$ |
| $z_f$ | $\infty$ | n/a |

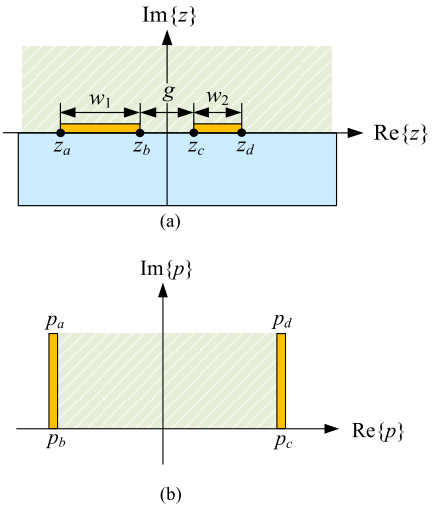


**FIGURE 14.** Schwarz-Christoffel transformation for the conventional CPS (Type 2): (a) $z$ -plane, (b) $p$ -plane.

where $\varepsilon_0$ is the dielectric constant of the air, and the modulus $k_1$ and the complementary modulus $k_1'$ are given as

$$k_1 = \sqrt{\frac{(z_d - z_c)(z_e - z_b)}{(z_d - z_b)(z_e - z_c)}}, \quad k_1{}' = \sqrt{1 - k_1^2} \tag{2}$$

*Type 2:* Type 2 is the analysis region for the upper half-plane (in the air) of an asymmetric CPS as shown in Fig. 14(a). The CPS consists of parallel signal and ground lines with linewidths of $w_1$ and $w_2$, respectively, and gap of $g$ in the $z$-plane. The parameters in the $z$-plane with the mapping angles are listed in Table 4. In a similar way to Type 1, the $z$-plane with the 90° mapping points at $z_a$, $z_b$, $z_c$, and $z_d$ is transformed into the $p$-plane in the form of a parallel plate (shown in Fig. 14(b)) using the Schwarz-Christoffel transformation [45]. With the parallel plate in the $p$-plane, the line capacitance $C_2$ of Type 2 is obtained as

$$C_2 = \varepsilon_0 \left| \frac{p_d - p_c}{p_d - p_a} \right| = \varepsilon_0 \frac{K(k_2')}{K(k_2)} \tag{3}$$

where the modulus $k_2$ and the complementary modulus $k_2'$ are expressed as

$$k_2 = \sqrt{\frac{(z_c - z_b)(z_d - z_a)}{(z_c - z_a)(z_d - z_b)}}, \quad k_2{}' = \sqrt{1 - k_2^2} \tag{4}$$

*Type 3:* Type 3 is the analysis region for the inner substrate (with relative dielectric constant $\varepsilon_r$) of an asymmetric CPS

**TABLE 4.** Parameters of Type 2 in the z-plane.

| Parameter | $z$-plane | Mapping angle |
|---|---|---|
| $z_a$ | $-w_1-g/2$ | $\pi/2$ |
| $z_b$ | $-g/2$ | $\pi/2$ |
| $z_c$ | $g/2$ | $\pi/2$ |
| $z_d$ | $w_2+g/2$ | $\pi/2$ |

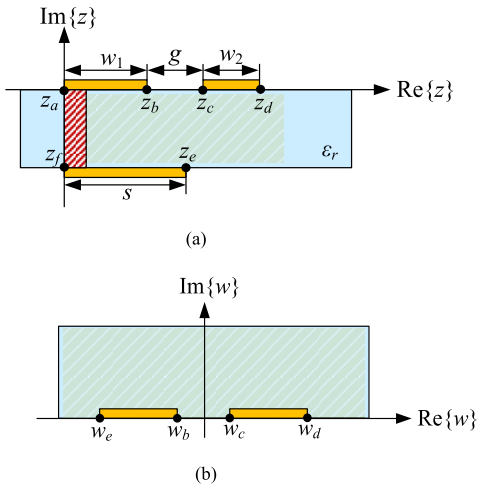


**FIGURE 15.** Asymmetric CPS with a finite ground plane (Type 3): (a) $z$ -plane, (b) $w$ -plane.

**TABLE 5.** Parameters of Type 3 in the z-plane.

| Parameter | $z$-plane | Mapping angle |
|---|---|---|
| $z_a$ | 0 | $\pi/2$ |
| $z_b$ | $w_1$ | n/a |
| $z_c$ | $w_1+g$ | n/a |
| $z_d$ | $w_1+g+w_2$ | n/a |
| $z_e$ | $s-jh$ | n/a |
| $z_f$ | $-jh$ | $\pi/2$ |

with a finite ground plane as shown in Fig. 15(a). The analysis Type 3 consists of a signal line, a top ground line, and a bottom ground line in the $z$-plane. The bottom ground line is connected to the top ground line by means of a ground wall (an array of vias). By changing the top linewidths $w_1$ and $w_2$, bottom linewidth $s$, and gap $g$, the line capacitance can be adjusted. The parameters in the $z$-plane with the mapping angles are listed in Table 5. When the width of the bottom ground line is small, the electric field line distribution of Type 3 is similar to that of the conventional CPS. Otherwise, it is similar to that of an MSL. Due to the one ground wall, the 90° mapping points (inside the substrate) are selected at the edge points of the ground wall. The $z$-plane with the 90° mapping points at $z_a$ and $z_f$ is transformed into the $w$-plane in the form of an asymmetric CPS, as shown in Fig. 15(b), using the Schwarz-Christoffel transformation of (5) and (6). From the analysis Type 2, the asymmetric CPS is transformed into a parallel plate in the $p$-plane. Therefore, the line capacitance

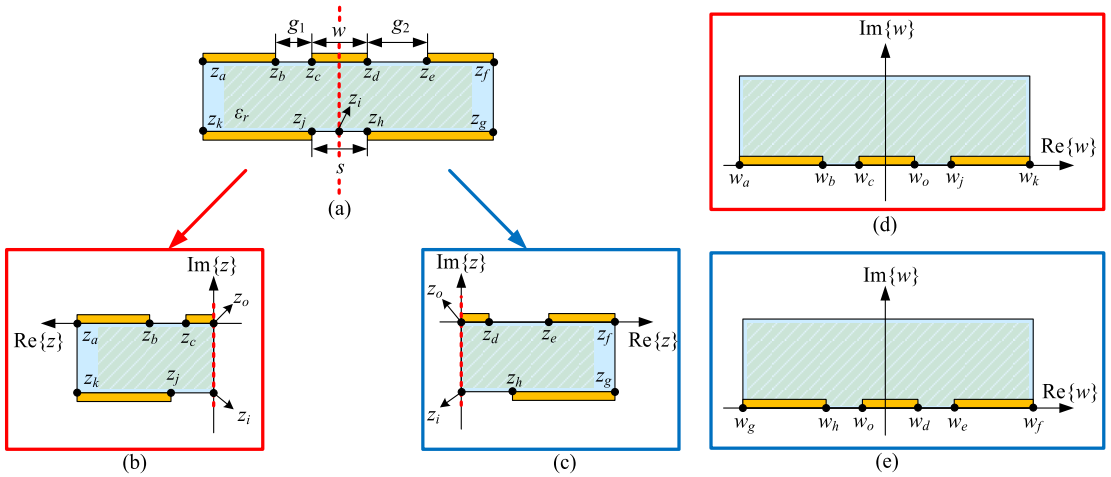


**FIGURE 16.** Internal region of a CBCPW with a ground aperture (Type 4): (a) configuration of Type 4 in the $z$ -plane, (b) left-side region in the $z$ -plane, (c) right-side region in the $z$ -plane, (d) left-side region in the $w$ -plane, (e) right-side region in the $w$ -plane.

$C_3$ of Type 3 can be expressed as (7).

$$z = \int \frac{h/\pi}{\sqrt{(w-1)(w+1)}} dw \tag{5}$$

$$w = \cosh(\pi z/h) \tag{6}$$

$$C_3 = \varepsilon_r \varepsilon_0 \frac{K(k_3')}{K(k_3)} \tag{7}$$

where the modulus $k_3$ and the complementary modulus $k_3'$ are given as

$$k_3 = \sqrt{\frac{(w_c - w_b)(w_d - w_e)}{(w_c - w_e)(w_d - w_b)}}, \quad k_3{}' = \sqrt{1 - k_3^2} \tag{8}$$

*Type 4:* Type 4 is the analysis region for the inner substrate region (with relative dielectric constant $\varepsilon_r$) of an asymmetric CBCPW with a ground aperture as shown in Fig. 16(a). The signal line with linewidth of $w$ is surrounded by the top-side ground planes with gaps $g_1$ and $g_2$, and there is a bottom ground plane with an aperture $s$ in the $z$-plane. The parameters in the $z$-plane with the mapping angles are listed in Table 6. As compared with Type 3, the line capacitance of Type 4 can be additionally modified by changing the bottom aperture. The line capacitance of Type 4 can be analyzed by dividing it into the left-side ($C_l$) and right-side ($C_r$) regions as shown in Figs. 16 (b) and (c), respectively. In Figs. 16 (b) and (c), each half region is identical to Type 3. Each half-plane region in the $z$-plane can be transformed into an asymmetric CPW in the $w$-plane using the Schwarz-Christoffel transformation with the 90° mapping points at $z_o$ and $z_i$ as shown in Figs. 16 (d) and (e). Then, by using the same process of Type 1, the line capacitances of the two regions are expressed in (9) with moduli $k_l$, $k_l'$, $k_r$, and $k_r'$, which are calculated using (10) and (11). The total line capacitance $C_4$ of Type 4 is obtained as (12).

$$C_l = \varepsilon_r \varepsilon_0 \frac{K(k_l)}{K(k_l')}, \qquad C_r = \varepsilon_r \varepsilon_0 \frac{K(k_r)}{K(k_r')} \tag{9}$$

**TABLE 6.** Parameters of Type 4 in the z-plane.

| Parameter | $z$-plane | Mapping angle |
|---|---|---|
| $z_o$ | 0 | $\pi/2$ |
| $z_a$, $z_f$, $z_g$, $z_k$ | $\infty$ | n/a |
| $z_b$ | $g_1$+$w/2$ | n/a |
| $z_e$ | $g_2$+$w/2$ | n/a |
| $z_c$, $z_d$ | $w/2$ | n/a |
| $z_h$, $z_j$ | $s/2-jh$ | n/a |
| $z_i$ | $-jh$ | $\pi/2$ |

$$k_l = \sqrt{\frac{(w_o - w_c)(w_j - w_b)}{(w_o - w_b)(w_j - w_c)}}, \quad k_l{}' = \sqrt{1 - k_l^2} \tag{10}$$

$$k_r = \sqrt{\frac{(w_d - w_o)(w_e - w_h)}{(w_d - w_h)(w_e - w_o)}}, \quad k_r{}' = \sqrt{1 - k_r^2} \tag{11}$$

$$C_4 = C_l + C_r \tag{12}$$

*Type 5:* Type 5 is the analysis region for the fringing field lines existing mostly in the air as shown in Fig. 17(a). The electric field of Type 5 is distributed in a similar way to Type 3 in the $z$-plane. The parameters in the $z$-plane with the mapping angles are listed in Table 7. If the bottom ground width is larger than $w_1 + g\text{-}h/\pi$, only a portion of the top conductor (from $z_b$ to $z_a$) is used for the fringing field calculation. Also, due to the overlapped width between top and bottom conductors, the edge point $z_d$ on the bottom ground plane is located at distance $h/\pi$ from $z_c$. On the other hand, if the bottom ground width is smaller than $w_1 + g\text{-}h/\pi$, the entire top conductor with linewidth $w_2$ is used for the fringing field calculation. In this case, the edge point $z_d$ on the bottom ground plane is located at distance $w_2 + g\text{-}s$ from $z_c$ [46]. By using the Schwarz-Christoffel transformation, the structure with 90° and 270° mapping angles at $z_a$ and $z_c$, respectively, in the $z$-plane is mapped into an asymmetric CPS line in the $w$-plane

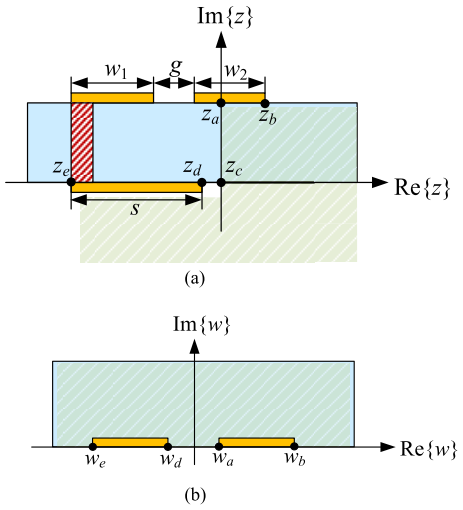


**FIGURE 17.** Fringing fields outside the substrate (Type 5): (a) $z$ -plane, (b) $w$ -plane.

**TABLE 7.** Parameters of Type 5 in the z-plane.

| Parameter | $z$-plane | Mapping angle |
|---|---|---|
| $z_a$ | $jh$ | $\pi/2$ |
| $z_b$ | $w_1+w_2+g-s-h/\pi+jh$ where $s>w_1+g-h/\pi$<br>$w_2$ where $s<w_1+g-h/\pi$ | n/a |
| $z_c$ | 0 | $3/2\pi$ |
| $z_d$ | $-h/\pi$ where $s>w_1+g-h/\pi$<br>$-w_1-g+s$ where $s<w_1+g-h/\pi$ | n/a |
| $z_e$ | $-s-z_d$ | n/a |

as shown in Fig. 17(b).

$$z = \int \frac{h}{\pi}\sqrt{\frac{(w+1)}{(w-1)}}dw \tag{13}$$

$$z = \frac{h}{\pi}\left[\sqrt{w^2-1}+\ln(w+\sqrt{w^2-1})\right]+jh \tag{14}$$

$$C_5 = \varepsilon_0\frac{K(k_5')}{K(k_5)} \tag{15}$$

$$k_5 = \sqrt{\frac{(w_a-w_d)(w_b-w_e)}{(w_a-w_e)(w_b-w_d)}}, \quad k_5' = \sqrt{1-k_5^2} \tag{16}$$

where $k_5$ and $k_5'$ are the moduli. Using the inverse relation of (14), which is derived from (13), an asymmetric CPS is transformed into a parallel plate. Therefore, the line capacitance $C_5$ of Type 5 is obtained as (15).

*Type 6:* Type 6 is the analysis region outside of a CBCPW with a ground aperture as shown in Fig. 18(a). The bottom aperture $s$ allows to generate fringing fields outside the substrate (in the $z$-plane) in a similar way to Type 5. The parameters in the $z$-plane with the mapping angles are listed in Table 8. By considering only vertical electric field lines within the substrate, the analysis region of Type 6 (Fig. 18(a)) can be divided into two analysis regions (gray color) by introducing an image plate with a linewidth $w'$ as shown in Fig. 18(b). When the bottom ground aperture width is smaller

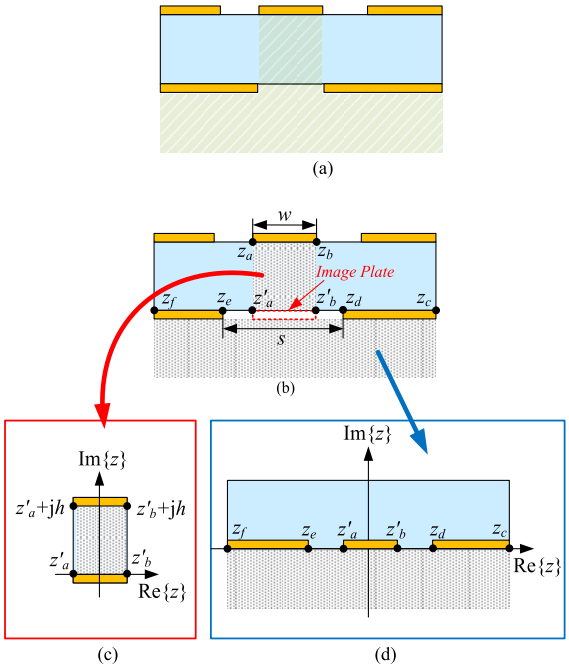


**FIGURE 18.** External region of the CBCPW with a ground aperture (Type 6): (a) configuration of Type 6, (b) $z$ -plane, (c) parallel plate region in the $z$ -plane, (d) conventional CPW region in the $z$ -plane.

**TABLE 8.** Parameters of Type 6 in $z$ plane.

| Parameter | $z$-plane | Mapping angle |
|---|---|---|
| $z_a$ | $-w/2+jh$ | n/a |
| $z_b$ | $w/2+jh$ | n/a |
| $z_a'$ | 0 where $s<2h/\pi$<br>$-s/2+h/\pi$ where $s<w+2h/\pi$<br>$-w/2$ where $s>w+2h/\pi$ | $\pi/2$ |
| $z_b'$ | $-z_a'$ | $\pi/2$ |
| $z_c$ | $\infty$ | n/a |
| $z_d$ | $s/2$ | $\pi/2$ |
| $z_e$ | $-s/2$ | $\pi/2$ |
| $z_f$ | $-\infty$ | n/a |

than $2h/\pi$, introduction of an image plate is not needed since the electric field lines are mostly contained inside the substrate. However, if the aperture width $s$ is greater than $2h/\pi$ and less than $w+2h/\pi$, an image plate with $w' = s-2h/\pi$ is used. Also, if the aperture width is larger than $w+2h/\pi$, an image plate with $w' = w$ (linewidth of the signal line) is introduced. From Fig. 18(c), the line capacitance $C_p$ between the signal line and image plate is obtained as (17). In addition, since the analysis region under the substrate (Fig. 18(d)) is that of a conventional CPW (Type 1), the line capacitance $C_c$ is expressed as (18) with the moduli $k_7$ and $k_7'$ in (19). Therefore, the total line capacitance $C_6$ of Type 6 is obtained as a series connection of two capacitances [40].

$$C_p = \varepsilon_0\frac{w'}{h} \quad \text{where } w' = z_b' - z_a' \tag{17}$$

$$C_c = \varepsilon_0\frac{K(k_6)}{K(k_6')} \tag{18}$$

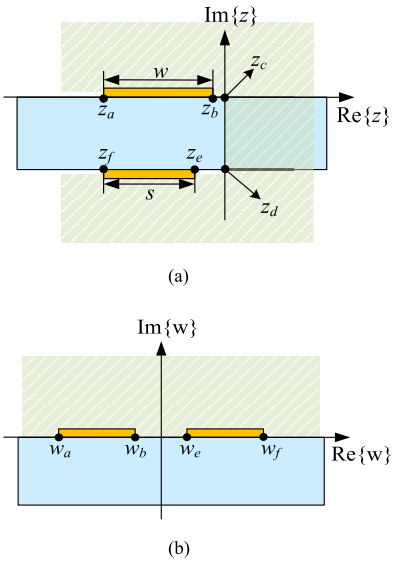


**FIGURE 19.** Fringing fields of a PSL (Type 7): (a) $z$ -plane, (b) $w$ -plane.

**TABLE 9.** Parameters of Type 7 in the z-plane.

| Parameter | $z$-plane | Mapping angle |
|---|---|---|
| $z_a$ | $-w-h/\pi$ | n/a |
| $z_b$ | $-h/\pi$ | n/a |
| $z_c$ | 0 | $3/2\pi$ |
| $z_d$ | $-jh$ | $3/2\pi$ |
| $z_e$ | $-w+s-h/\pi-jh$ | n/a |
| $z_f$ | $-w-h/\pi-jh$ | n/a |

$$k_6 = \sqrt{\frac{(z_b' - z_a')(z_d - z_e)}{(z_b' - z_e)(z_d - z_a')}}, \quad k_6' = \sqrt{1 - k_6^2} \tag{19}$$

$$C_6 = \frac{C_p C_c}{C_p + C_c} \tag{20}$$

*Type 7:* Type 7 is the analysis region for the fringing field shown in Fig. 19(a). Since most of the analysis region resides outside the substrate, this analysis region can be approximated as an air-only region, neglecting the field lines inside the thin dielectric substrate. The linewidths (in the $z$-plane) of the top signal conductor and the bottom ground conductor are $w$ and $s$, respectively. The parameters in the $z$-plane with the mapping angles are listed in Table 9. In this analysis type, the two 270° mapping angles at $z_c$ and $z_d$ are used to transform an asymmetric parallel plate in the $z$-plane into an asymmetric CPS line in the $w$-plane as shown in Fig 19(b). Using a relation between the $z$-plane and $w$-plane in (21), the parameters in the $w$-plane can be obtained as the inverse relation of (22). The line capacitance $C_7$ of Type 7 is calculated by (23) with the modulus $k_7$ and the complementary modulus $k_7'$ in (24).

$$z = \int \sqrt{(w-1)(w+1)}dw \tag{21}$$

$$z = \frac{h}{\pi}\left[w\sqrt{w^2-1} - \ln(w + \sqrt{w^2-1})\right] - jh \tag{22}$$

$$C_7 = \varepsilon_0 \frac{K(k_7')}{K(k_7)} \tag{23}$$

$$k_7 = \sqrt{\frac{(w_e - w_b)(w_f - w_a)}{(w_e - w_a)(w_f - w_b)}}, \quad k_7' = \sqrt{1 - k_7^2} \tag{24}$$

### C. CHARACTERISTIC LINE IMPEDANCE

The characteristic line impedance of each cross-sectional model (Model I – IV) can be calculated by combining the line capacitance of each analysis region. If a cross-sectional model consists of three analysis regions, $C_{\mathrm{I}}$, $C_{\mathrm{II}}$, or $C_{\mathrm{III}}$ represents the line capacitance of Regions 1-3, respectively. Then, the characteristic line impedance can be obtained by using (25), and the effective permittivity $\varepsilon_{eff}$ can be expressed as (26), where $C_{\mathrm{I}}'$, $C_{\mathrm{II}}'$, and $C_{\mathrm{III}}'$ are the capacitances with air filling.

$$Z = \frac{120\pi}{\sqrt{\varepsilon_{eff}}(C_{\mathrm{I}}' + C_{\mathrm{II}}' + C_{\mathrm{III}}')/\varepsilon_0} \tag{25}$$

$$\varepsilon_{eff} = \frac{C_{\mathrm{I}} + C_{\mathrm{II}} + C_{\mathrm{III}}}{C_{\mathrm{I}}' + C_{\mathrm{II}}' + C_{\mathrm{III}}'} \tag{26}$$

For the optimal impedance matching, the characteristic line impedance values along the transition length can be specified. Then, the design parameters to attain the specific characteristic line impedance at a certain location of the transition can be obtained by an inverse relation of (25).

In Table 10, for each cross-sectional model of the transition, the corresponding analysis types are summarized with the analytical expressions of the characteristic line impedance and effective dielectric constant.

*Model I (Fig. 9):* Model I consists of three analysis regions, and can be analyzed by the corresponding analysis types (Type 1, Type 4, and Type 6); i.e., the characteristic line impedance of the Model I can be obtained by summing up the line capacitances of these analysis types. Region I (in the air) is Type 1, and Region II is Type 4 (inner region of the dielectric medium). Region III consists of the substrate and the air area outside the substrate, and can be analyzed by using the analysis Type 6 in air.

*Model II (Fig. 10):* Model II consists of four analysis regions. Each analysis region of the Model II is distributed either in the air or inside the substrate. Region I is the half-plane (in the air) of a conventional CPS, and can be analyzed by Type 2. Region II indicates the analysis region of electric field lines inside the substrate, and the line capacitance can be obtained by the analysis Type 3. The fringing fields of Region III are distributed in both the substrate and air, and the line capacitance can be approximately obtained using the analysis Type 5 in air. When the bottom ground width is larger than $2w + g$, however, the additional fringing fields (of Type 7 in the air), which originate from the top conductor, pass through the dielectric, and hoop back to the bottom ground plane, can occur at the side region as shown in Fig. 20.

**TABLE 10. Characteristic impedances and effective dielectric constants of the cross-sectional Models I-IV.**

| Model | Corresponding Analysis Types | | | Characteristic Line Impedance $Z_0$ | Effective Dielectric Constant $\varepsilon_{eff}$ |
|---|---|---|---|---|---|
| | Region | Type | Analysis Area | | |
| I | I | 1 | Air | $\frac{120\pi}{\sqrt{\varepsilon_{eff}}(C_1+C_4'+C_6)/\varepsilon_0}$ | $\frac{C_1+C_4+C_6}{C_1+C_4'+C_6}$ |
| | II | 4 | Substrate | | |
| | III | 6 | Air | | |
| II | I | 2 | Air | $\frac{120\pi}{\sqrt{\varepsilon_{eff}}(C_2+C_3'+C_5+C_7)/\varepsilon_0}$ | $\frac{C_2+C_3+C_5+C_7}{C_2+C_3'+C_5+C_7}$ |
| | II | 3 | Substrate | | |
| | III | 5 | Air | | |
| | IV | 7 | Air | | |
| III | I (Left) | 5 | Air | $\frac{120\pi}{\sqrt{\varepsilon_{eff}}(\varepsilon_0 w/h+C_{5r}+C_{7r}+C_{5l}+C_{7l})/\varepsilon_0}$ | $\frac{\varepsilon_0\varepsilon_r w/h+C_{5r}+C_{7r}+C_{5l}+C_{7l}}{\varepsilon_0 w/h+C_{5r}+C_{7r}+C_{5l}+C_{7l}}$ |
| | I (Right) | 5 | Air | | |
| | II | - | Substrate | | |
| | III (Left) | 7 | Air | | |
| | III (Right) | 7 | Air | | |
| IV | I | 4 | Air | $\frac{120\pi}{\sqrt{\varepsilon_{eff}}(C_{4(I)}+C_{4(II)}'+C_6)/\varepsilon_0}$ | $\frac{C_{4(I)}+C_{4(II)}+C_6}{C_{4(I)}+C_{4(II)}'+C_6}$ |
| | II | 4 | Substrate | | |
| | III | 6 | Air | | |

$\varepsilon_0$: air permittivity, $\varepsilon_r$: relative permittivity, $w$: signal linewidth in Model III, $h$: substrate height, $C_{4(I)}$: capacitance of Type 4 in Region I of Model IV, $C_{4(II)}$: capacitance of Type 4 in Region II of Model IV, $C_{5r}$: capacitance of Type 5 in the right Region II of Model III, $C_{5l}$: capacitance of Type 5 in the left Region II of Model III, $C_{7r}$: capacitance of Type 7 in the right Region II of Model III, $C_{7l}$: capacitance of Type 7 in the left Region II of Model III.

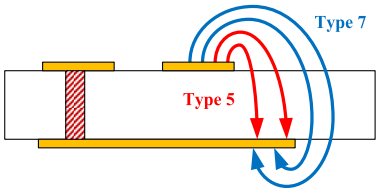


**FIGURE 20. Side fringing field of Model II.**

*Model III (Fig. 11):* Unlike other cross-sectional models, the analysis regions of the Model III are divided horizontally into the left, center, and right areas. Region II is a parallel plate area within a substrate. Region I and Region III represent analysis regions with left and right fringing fields, respectively. The fringing fields in Region I and Region III are composed of Type 5 and Type 7 in the air. When the bottom ground linewidth is larger than the top signal linewidth, the amount of the Type 5 electric fields increases. When the bottom ground linewidth is smaller than the top signal linewidth, the amount of the Type 7 electric fields increases as the amount of the Type 5 electric fields simultaneously decreases. In each side region, two types of fringing fields coexist.

*Model IV (Fig. 12):* In Model IV, the conductor walls are placed at the boundaries of the Model I for electric shielding, where the top and bottom areas are filled with the air. Region I (identical to Type 4) is an air-filled region, and Region II is equal to Region I with a dielectric-filled medium. Region III is identical to Type 6. Note that there exists an overlapped analysis region between the Type 4 and Type 6. With a thin substrate, the electric field lines of Region III are assumed to be mostly distributed in the air, and thus the line capacitance of Region III is estimated mainly by field lines distributed in the air.

***Accuracy Verification of Analytical Formulas:*** The estimated characteristic line impedances using the analytical formulas (solid line) and using 3D EM simulations (CST Microwave Studio: dotted line) are compared for the proposed four cross-sectional models. The calculated and simulated characteristic line impedances of four cross-sectional models with varying the ground aperture $a$ or ground linewidth $s$ are shown in Figs. 21 - 24. Here, the substrates with different dielectric constants (2.2, 4.3, and 10.2) are considered. When a high permittivity substrate is used, the characteristic line impedance becomes reduced since the electric field lines are more concentrated within the substrate.

In Fig. 21(a), the characteristic line impedance of Model I for a symmetric structure with gap width ($g_1$ and $g_2$) of 5 mil is shown. The average error/deviation between the calculated and simulated results is within 5.8% (3.4 Ω) in the case of the lowest dielectric constant of 2.2, while lesser error/deviation values are obtained with higher permittivity substrates. In Fig. 21(b), the characteristic line impedance of Model I for an asymmetric gap case ($g_1 = 5$ mil, $g_2 = 30$ mil) is shown. The results show a similar trend to the symmetric case. The average error/deviation at the lowest dielectric constant of 2.2 is within 3.0% (1.4 Ω).

The characteristic line impedance of Model II for a symmetric case with linewidth ($w_1$ and $w_2$) of 15 mil is shown in Fig. 22(a). The deviation between the calculated and simulated values slightly decreases by using high permittivity substrates due to more concentrated field lines within the substrate. The average error/deviation is within 3.3% (3.4 Ω) with dielectric constant of 2.2. However, with a narrow (bottom) ground plane (i.e., $s < 10$ mil), the error/deviation

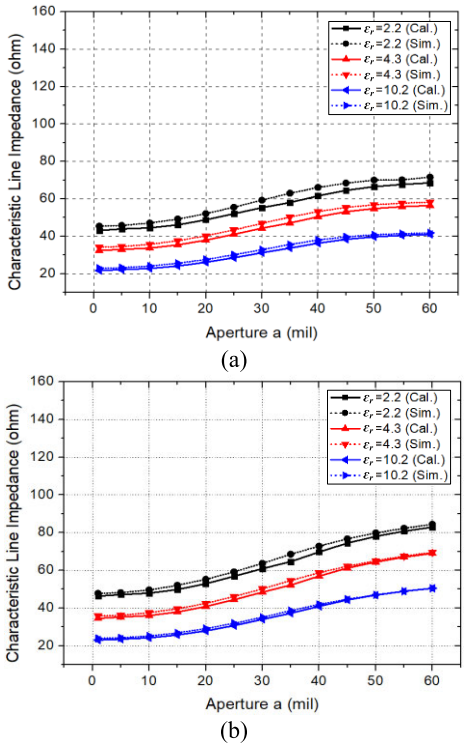


**FIGURE 21.** Calculated and EM-simulated characteristic line impedances of Model I with varying the ground aperture a: (a) symmetric structure (w = 30 mil,$g_1 = g_2 = 5$ mil), (b) asymmetric structure (w = 30 mil, $g_1 = 5$ mil, $g_2 = 30$ mil).

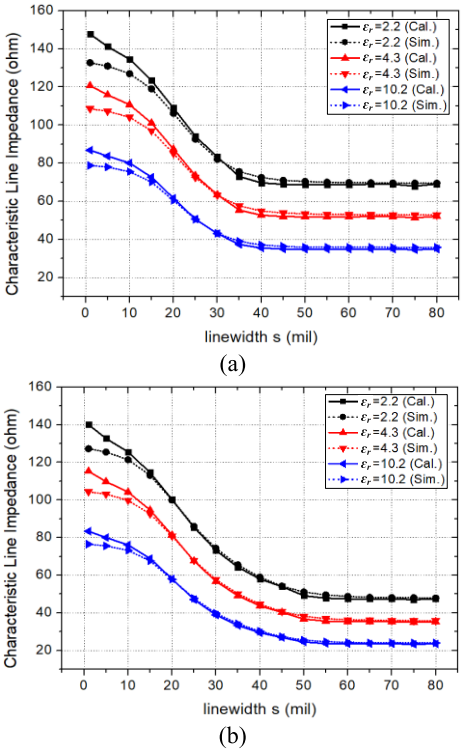


**FIGURE 22.** Calculated and EM-simulated characteristic line impedances of Model II with varying the ground linewidth s: (a) symmetric structure ( $w_1 = w_2 = 15$ mil andg = 5 mil), (b) asymmetric structure ( $w_1 = w_2 = 30$ mil andg = 5 mil).

increases to 11.4% (15.1 Ω) due to formation of the conventional CPS mode as shown in Fig. 23. An asymmetric case of Model II is shown in Fig. 22(b). The linewidths $w_1$ and $w_2$ are 15 mil and 30 mil, respectively. The average error/deviation is within 2.5% (2.2 Ω) with dielectric constant of 2.2.

The characteristic line impedance of Model III is calculated as changing the signal linewidth $w$ (15 mil and 45 mil) as shown in Figs. 24 (a) and (b). As the linewidth $w$ becomes increased, the effect of side fringing fields tends to be reduced since the electric field lines tend to be mostly contained within the substrate. Figs. 24 (a) and (b) show that the average error/deviation between the calculated and simulated results are within 2.7% (2.4 Ω) and 0.9% (0.4 Ω), respectively, with dielectric constant of 2.2.

The characteristic line impedance of Model IV for a symmetric structure with the ground aperture width ($g_1$ and $g_2$) of 5 mil is plotted in Fig. 25 (a). In a similar way to the Model I, the line impedance result shows the maximum error/deviation within 4.7% (2.4 Ω) when using a substrate of the lowest dielectric constant of 2.2 as shown in Fig. 25(a). Also, the characteristic line impedance curves become flattened when $s > 80$ mil. In Fig. 25(b), the characteristic line impedance of the Model IV for an asymmetric case with ground aperture width ($g_1$ and $g_2$) of 5 mil and 40 mil is shown. The result again shows a similar trend with the symmetric case. The maximum error/deviation is within 3.8% (2.3 Ω) with dielectric constant of 2.2.

It is important to note that there may be some overlapped regions for the analysis Types such as the analysis Type 4 and Type 6 in Model I. The overlapped electric field lines inside the dielectric substrates cause to increase the total sum of the line capacitance, thus resulting in decrease of the calculated characteristic line impedance. Depending on the substrate permittivity and design parameters, the amount of error/deviation due to these overlapped regions in the calculated line impedance values using the analytic formulas can be as high as 5.8 %. In most practical cases, however, the planar transition designs based on the proposed analytical formulas result in ultra-wideband performance with low-insertion loss, obviating parameter tuning efforts.

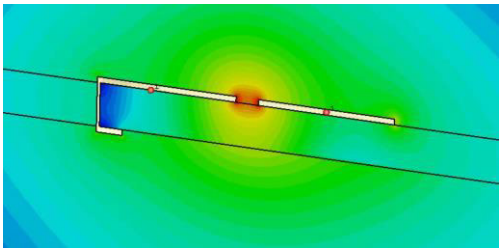

**FIGURE 23.** Conventional CPS mode of Model II with a narrow bottom ground plane.

### D. TRANSITION DESIGN

A practical and efficient design method for ultra-wideband planar transitions is proposed to connect any pair combination of TEM/quasi-TEM-type planar transmission lines. Each transmission line has a different range of characteristic line impedance. If the target transmission lines have different line impedance values, then the transition should function as

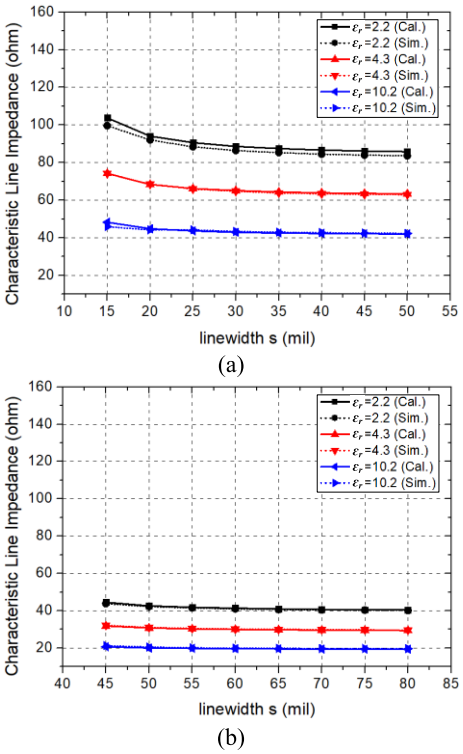


**FIGURE 24.** Calculated and EM-simulated characteristic line impedances of Model III with varying the ground linewidth s: (a) w = 15 mil, (b)w = 45 mil.

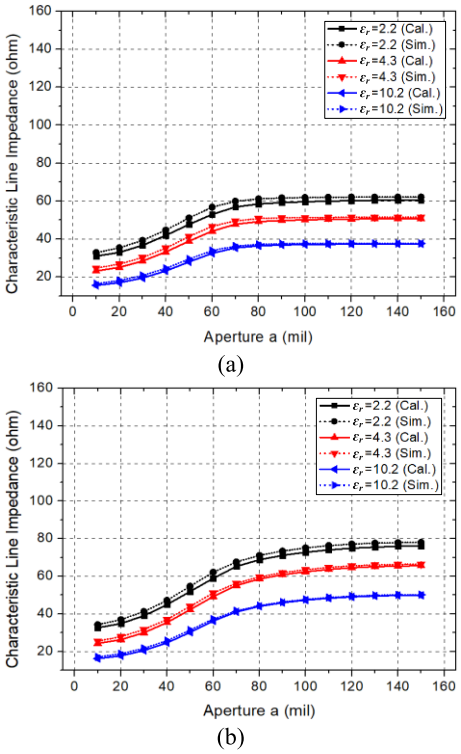


**FIGURE 25.** Calculated and EM-simulated characteristic line impedances of Model IV with varying the ground aperture a: (a) symmetric structure (w = 50 mil, $g_1 = g_2 = 5$ mil, $s_t = 50$ mil), (b) asymmetric structure (w = 50 mil, $g_1 = 5$ mil, $g_2 = 40$ mil, $s_t = 50$ mil).

an impedance transformer. In order to match the characteristic impedance between the two transmission lines, an impedance taper is required to minimize return loss. In order to maximize the operating frequency bandwidth, an optimal impedance taper such as the Klopfenstein taper can be used [41]. On the other hand, when the line impedances of the two transmission lines happen to be the same, a transition is designed to maintain at a constant line impedance throughout the transition for the maximum transition performance. The performances (operating bandwidth, return loss, and insertion loss) of various impedance tapering types are well analyzed in the literature [41], [42]. Here, the transition length determines the start operating frequency; i.e., a longer transition length is required to attain a lower operating frequency.

Once the target line impedance values along the transition are specified, the design parameters of the cross-sectional models (Model I to IV), such as the widths of the signal line(s) and ground line(s) (or ground plane(s)), gap width between the signal and ground line(s), and aperture width of the ground plane, can be efficiently determined using the analytical formulas based on the conformal mapping. If multiple parameters can be adjusted to attain the same line impedance, one parameter is chosen to form a simple shape, and the other parameters can be adjusted to attain the required line impedance. For example, if the signal linewidth and ground linewidth are design parameters, the width of signal line on the top side can be shaped linearly, and the ground linewidth is calculated to attain the required line impedance value using the analytical formulas.

Also, each transmission line has unique field line configurations. In addition to the impedance matching, the transition should smoothly transform electric field lines from one transmission line to another without abrupt shape changes.

The design technique proposed in this paper has been extensively verified to provide ultra-wideband performance with excellent characteristics as reported in [38]–[42]. The planar transitions implemented with the proposed design method have proven to work for several 10's of GHz bandwidth. When the characteristic line impedance difference between the two transmission lines is not very large, the transition can be designed to operate from near DC [39], [40].

## III. CONCLUSION

In this paper, a generalized technique to design a planar transition for any pair of planar transmission lines supporting TEM or quasi-TEM modes is proposed. The proposed design technique is based on the conformal mapping method, and analytical design formulas for the cross-sectional areas throughout the transition are used to form high-performing planar transitions. For the systematic analysis, cross-sectional structures among various planar transitions are categorized into four cross-sectional models. Also, to efficiently calculate the characteristic line impedance of a cross-sectional model, seven analysis types are identified. The line capacitances corresponding to the seven analysis types are derived in analytic formulas, and therefore the

characteristic line impedance of each cross-sectional model can be obtained as a sum of capacitances corresponding to analysis types with appropriate design parameters.

Characteristic line impedances of the four cross-sectional models with various design parameters can be calculated accurately, mostly well within 6% error. Due to some limitations of the proposed models, especially related to the actual line modes and overlapped region, the line impedance error can be as high as 10%. In most practical cases, however, the proposed planar transition designs based on the analytical formulas result in ultra-wideband performance with low-insertion loss. At least, the proposed transition design can produce a good initial design prototype for further optimization.

Therefore, the proposed planar transition design technique can be applied for various multi-layered packaging and MMICs, which can handle multi-GHz digital and analog data for the $5^{th}$ (and beyond $5^{th}$) generation mobile communications.

## REFERENCES

[1] D. Mirshekar-Syahkal, D. J. Newson, D. Wake, and I. D. Henning, "Wideband transitions for applications in MMIC's and OEIC's," *IEEE Microw. Guided Wave Lett.*, vol. 4, no. 9, pp. 299–300, Sep. 1994.

[2] D. Prieto, J. C. Cayrout, J. L. Cazaux, T. Parra, and J. Graffeuil, "CPS structure potentialities for MMICs: A CPS/CPW transition and a bias network," in *IEEE MTT-S Int. Microw. Symp. Dig.*, vol. 1, Jun. 1998, pp. 111–114.

[3] A. Bessemoulin, C. Gaessler, P. Marschall, and P. Quentin, "A chip-scale packaged amplifier MMIC using broadband hot-via transitions," in *Proc. 33rd Eur. Microw. Conf.*, vol. 1, Oct. 2003, pp. 289–292.

[4] V. Hurm, R. Weber, A. Tessmann, H. Massler, A. Leuther, M. Kuri, M. Riessle, H. P. Stulz, M. Zink, M. Schlechtweg, O. Ambacher, and T. Narhi, "A 243 GHz LNA module based on mHEMT MMICs with integrated waveguide transitions," *IEEE Microw. Wireless Compon. Lett.*, vol. 23, no. 9, pp. 486–488, Sep. 2013.

[5] A. Aljarosha, A. U. Zaman, and R. Maaskant, "A wideband contactless and bondwire-free MMIC to waveguide transition," *IEEE Microw. Wireless Compon. Lett.*, vol. 27, no. 5, pp. 437–439, May 2017.

[6] J. M. Perez-Escudero, A. E. Torres-Garcia, R. Gonzalo, and I. Ederra, "A Chebyshev transformer-based microstri-to-groove-gap-waveguide inline transition for MMIC packaging," *IEEE Trans. Compon., Packag., Manuf. Technol.*, vol. 9, no. 8, pp. 1595–1602, Aug. 2019.

[7] Y. Fan, B. L. Ooi, and L. M. Seng, "Compact CPW-to microstrip transition design for MMIC packaging," in *Proc. 7th Int. Symp. Antennas, Propag. EM Theory*, Oct. 2006, pp. 1–4.

[8] M. Sarkar and A. Majumder, "A novel broadband microstrip to waveguide transition at W band with high manufacturing tolerance suitable for MMIC packaging," in *IEEE MTT-S Int. Microw. Symp. Dig.*, Nov. 2018, pp. 1–4.

[9] K. Leong, W. R. Deal, V. Radisic, X. Bing Mei, J. Uyeda, L. Samoska, A. Fung, T. Gaier, and R. Lai, "A 340–380 GHz integrated CB-CPW-to-waveguide transition for sub millimeter-wave MMIC packaging," *IEEE Microw. Wireless Compon. Lett.*, vol. 19, no. 6, pp. 413–415, Jun. 2009.

[10] I. Ju, I.-B. Yom, and S.-H. Oh, "Novel vertical transition using a trough line, a slab line and shielded multilayer coplanar waveguides for 50 GHz LTCC hermetic SMT MMIC package," in *Proc. Eur. Microw. Conf.*, Oct. 2007, pp. 1361–1364.

[11] G. Lee, B. Lee, J.-Y. Jeong, and J. Lee, "Ka-band surface-mount cross-coupled SIW filter with multi-layered microstrip-to-GCPW transition," *IEEE Access*, vol. 7, pp. 66453–66462, May 2019.

[12] Z. Guo and T. Yang, "Novel compact ultra-wideband bandpass filter based on vialess vertical CPW/microstrip transitions," *Electron. Lett.*, vol. 53, no. 18, pp. 1258–1260, Aug. 2017.

[13] J. Zhou, H. J. Qian, J. Ren, and X. Luo, "Reconfigurable wideband filtering balun with tunable dual-notched bands using CPW-to-slot transition and varactor-loaded shorted-slot," *IEEE Access*, vol. 7, pp. 36761–36771, Feb. 2019.

[14] Y.-G. Kim, S.-Y. Song, and K. W. Kim, "A compact wideband ring coupler utilizing a pair of transitions for phase inversion," *IEEE Microw. Wireless Compon. Lett.*, vol. 21, no. 1, pp. 25–27, Jan. 2011.

[15] W. Feng, W. Che, and K. Deng, "Compact planar magic-T using E-plane substrate integrated waveguide (SIW) power divider and slotline transition," *IEEE Microw. Wireless Compon. Lett.*, vol. 20, no. 6, pp. 331–333, Jun. 2010.

[16] H. Zhu, Z. Cheng, and Y. J. Guo, "Design of wideband in-phase and out-of-phase power dividers using microstrip-to-slotline transitions and slotline resonators," *IEEE Trans. Microw. Theory Techn.*, vol. 67, no. 4, pp. 1412–1424, Apr. 2019.

[17] J. Jeong, Y. Kwon, D. S. Deakin, J. H. Hong, and E. A. Sovero, "44 GHz waveguide-based power amplifier module using double antipodal finline transitions," *Electron. Lett.*, vol. 38, no. 3, pp. 128–129, Jan. 2002.

[18] L. Samoska, W. R. Deal, G. Chattopadhyay, D. Pukala, A. Fung, T. Gaier, M. Soria, V. Radisic, X. Mei, and R. Lai, "A submillimeter-wave HEMT amplifier module with integrated waveguide transitions operating above 300 GHz," *IEEE Trans. Microw. Theory Techn.*, vol. 56, no. 6, pp. 1380–1388, Jun. 2008.

[19] W. Mohyuddin, Y.-G. Kim, D. S. Woo, H. C. Choi, and K. W. Kim, "A compact wideband ring mixer utilizing a pair of PLANAR transitions for phase inversion," *Microw. Opt. Technol. Lett.*, vol. 56, no. 8, pp. 1919–1922, Aug. 2014.

[20] K.-P. Ma, Y. Qian, and T. Itoh, "Analysis and applications of a new CPW-slotline transition," *IEEE Trans. Microw. Theory Techn.*, vol. 47, no. 4, pp. 426–432, Apr. 1999.

[21] S.-J. Wu and T.-G. Ma, "A wideband slotted bow-tie antenna with reconfigurable CPW-to-slotline transition for pattern diversity," *IEEE Trans. Microw. Theory Techn.*, vol. 56, no. 2, pp. 327–334, Feb. 2008.

[22] Y. Li, Z. Zhang, W. Chen, and Z. Feng, "Polarization reconfigurable slot antenna with a novel compact CPW-to-slotline transition for WLAN application," *IEEE Antennas Wireless Propag. Lett.*, vol. 9, pp. 252–255, Mar. 2010.

[23] J. R. Brews, "Characteristic impedance of microstrip lines," *IEEE Trans. Microw. Theory Techn.*, vol. MTT-35, no. 1, pp. 30–34, Jan. 1987.

[24] D. Homentcovschi, "High accuracy formulas for calculation of the characteristic impedance of microstrip lines," *IEEE Trans. Microw. Theory Techn.*, vol. 43, no. 9, pp. 2132–2137, Sep. 1995.

[25] M. Gillick, I. D. Robertson, and J. S. Joshi, "An analytical method for direct calculation of e and H-field patterns of conductor-backed coplanar waveguides," *IEEE Trans. Microw. Theory Techn.*, vol. 41, no. 9, pp. 1606–1610, Sep. 1993.

[26] A. K. Verma, P. Singh, and L. Matekovits, "Strip-width and slot-gap dependent equivalent isotropic substrate and dispersion characteristics of asymmetric coplanar waveguide, symmetric coplanar," *IEEE Trans. Microw. Theory Techn.*, vol. 62, no. 10, pp. 2232–2241, Oct. 2014.

[27] J. S. McLean and T. Itoh, "Analysis of a new configuration of coplanar stripline," *IEEE Trans. Microw. Theory Techn.*, vol. 40, no. 4, pp. 772–774, Apr. 1992.

[28] H. A. Wheeler, "Transmission-line properties of parallel strips separated by a dielectric sheet," *IEEE Trans. Microw. Theory Techn.*, vol. MTT-13, no. 2, pp. 172–185, Mar. 1965.

[29] J. S. Rao and B. N. Das, "Analysis of asymmetric stripline by conformal mapping," *IEEE Trans. Microw. Theory Techn.*, vol. MTT-27, no. 4, pp. 299–303, Apr. 1979.

[30] E. Yamashita, M. Nakajima, and K. Atsuki, "Analysis method for generalized suspended striplines," *IEEE Trans. Microw. Theory Techn.*, vol. MTT-34, no. 12, pp. 1457–1463, Dec. 1986.

[31] Y.-H. Suh and K. Chang, "A wideband coplanar stripline to microstrip transition," *IEEE Microw. Wireless Compon. Lett.*, vol. 11, no. 1, pp. 28–29, Jan. 2001.

[32] R. N. Simons, N. I. Dib, and L. P. B. Katehi, "Coplanar stripline to microstrip transition," *Electron. Lett.*, vol. 31, no. 20, pp. 28–29, Sep. 1995.

[33] T. H. Lin, "Via-free broadband microstrip to CPW transition," *Electron. Lett.*, vol. 37, no. 15, pp. 960–961, Jul. 2001.

[34] X. Y. Zhang, J.-X. Chen, and Q. Xue, "Broadband transition between double-sided parallel-strip line and coplanar waveguide," *IEEE Microw. Wireless Compon. Lett.*, vol. 17, no. 2, pp. 103–105, Feb. 2007.

[35] C. H. Ahn and K. Chang, "Wideband coplanar stripline to double-sided parallel-strip line transition," *Electron. Lett.*, vol. 45, no. 14, pp. 748–749, Jul. 2009.

[36] D. Li, J. Xu, B. Zhang, W. Liu, and L. Du, "GCPW to stripline vertical transition for K-band applications in LTCC," in *Proc. Asia–Pacific Microw. Conf. (APMC)*, vol. 3, Dec. 2015, pp. 1–3.
[37] S.-G. Kim and K. Chang, "Ultrawide-band transitions and new microwave components using double-sided parallel-strip lines," *IEEE Trans. Microw. Theory Techn.*, vol. 52, no. 9, pp. 2148–2152, Sep. 2004.
[38] Y.-G. Kim, K. Wook Kim, and Y.-K. Cho, "An ultra-wideband microstrip-to-CPW transition," in *IEEE MTT-S Int. Microw. Symp. Dig.*, Jun. 2008, pp. 1079–1082.
[39] Y.-G. Kim and K. W. Kim, "Design of an ultra-wideband transition from double-sided parallel stripline to coplanar waveguide," *Int. J. Antennas Propag.*, vol. 2013, pp. 1–8, Jan. 2013.
[40] Y.-G. Kim and K. W. Kim, "A new design method for ultrawideband microstrip-to-suspended stripline transitions," *Int. J. Antennas Propag.*, vol. 2013, pp. 1–9, Jan. 2013.
[41] G. H. Lee, W. Mohyuddin, H. C. Choi, and K. W. Kim, "Asymmetric ultra-wideband microstrip-to-coplanar stripline transition," *IEEE Microw. Wireless Compon. Lett.*, vol. 28, no. 5, pp. 386–388, May 2018.
[42] G. H. Lee, D. H. Kim, W. Mohyuddin, S. Kumar, H. C. Choi, and K. W. Kim, "Design of an ultra-wideband coplanar strip-to-parallel stripline transition using an analytical model based on conformal mapping," *Microw. Opt. Technol. Lett.*, vol. 63, no. 4, pp. 1054–1060, Apr. 2021.
[43] Y.-G. Kim and K. W. Kim, "Analysis of coplanar waveguide with a bottom ground aperture," *IEEE Microw. Wireless Compon. Lett.*, vol. 22, no. 11, pp. 550–552, Nov. 2012.
[44] C. P. Wen, "Coplanar waveguide: A surface strip transmission line suitable for nonreciprocal gyromagnetic device applications," *IEEE Trans. Microw. Theory Techn.*, vol. MTT-17, no. 12, pp. 1087–1090, Dec. 1969.
[45] G. Ghione, "A CAD-oriented analytical model for the losses of general asymmetric coplanar lines in hybrid and monolithic MICs," *IEEE Trans. Microw. Theory Techn.*, vol. 41, no. 9, pp. 1499–1510, Sep. 1993.
[46] N. Pesonen, W. K. Kahn, R. A. Allen, M. W. Cresswell, and M. E. Zaghloul, "Application of conformal mapping approximation techniques: Parallel conductors of finite dimensions," *IEEE Trans. Instrum. Meas.*, vol. 53, no. 3, pp. 812–821, Jun. 2004.

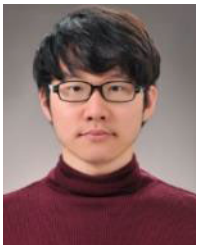

**GWAN HUI LEE** (Student Member, IEEE) received the B.S. degree in physics and energy sciences and the M.S. degree in electronics engineering from Kyungpook National University, Daegu, South Korea, in 2015 and 2017, respectively, where he is currently pursuing the Ph.D. degree in electronics engineering (specializing in radio communication systems engineering) with the Microwave Communications Laboratory. His research interests include design and development of microwave circuits and wideband microwave passive components.

**SACHIN KUMAR** received the B.Tech. degree in electronics and communication engineering from Uttar Pradesh Technical University, Lucknow, India, in 2009, and the M.Tech. and Ph.D. degrees in electronics and communication engineering from Guru Gobind Singh Indraprastha University, Delhi, India, in 2011 and 2016, respectively. He is currently working as a Postdoctoral Researcher with the School of Electronic and Electrical Engineering, Kyungpook National University, Daegu, South Korea. His research interests include circularly-polarized microstrip antennas, reconfigurable antennas, ultra-wideband antennas, defected ground structure, and microwave components.

**WAHAB MOHYUDDIN** (Member, IEEE) received the B.S. degree in telecommunication engineering from the National University of Computer and Emerging Sciences, Pakistan, in 2011, and the M.S. and Ph.D. degrees in electronics engineering from Kyungpook National University, Daegu, South Korea, in 2014 and 2018, respectively. He served as a Postdoctoral Researcher with the Microwave Convergence Laboratory, Kyungpook National University, for a year. He is currently an Assistant Professor with the National University of Sciences and Technology, Pakistan. He has authored and coauthored of several peer-reviewed journal and conference papers. His research interests include design of RF/microwave/millimeter-wave circuits and systems designing, wideband microwave passive components, frequency selective surfaces, and microwave antennas.

**HYUN CHUL CHOI** received the B.S. degree in electronics engineering from Kyungpook National University, Daegu, South Korea, in 1982, and the M.S. and Ph.D. degrees in electronics engineering from the Korea Advanced Institute of Science and Technology (KAIST), South Korea, in 1984 and 1989, respectively. In 1990, he joined Kyungpook National University as a Professor and served as the Dean of the IT College. He has published numerous articles in the fields of EMI/EMC, scattering and propagation station, and RF/microwave circuits and systems.

**KANG WOOK KIM** (Member, IEEE) received the B.S. and M.S. degrees in electrical engineering from Seoul National University, South Korea, in 1985 and 1987, respectively, and the Ph.D. degree in electrical engineering from the University of California at Los Angeles, Los Angeles, CA, USA, in 1996. In 1987, before pursuing his Ph.D. degree, he worked as a Researcher with the Korea Electrotechnology Research Institute. He worked as a Design Engineer with P-Com Inc., USA, and Narda DBS Microwave, USA, in 1998 and 1999, respectively. In 2001, he joined as a Faculty Member with the School of Electronics Engineering, Kyungpook National University, Daegu, South Korea. He is currently a Founder of EM-wise Communications Company Inc., South Korea. His research interests include microwave communication system and subsystems, microwave/mm-wave ultra-wideband components and packaging, wireless communications, and microwave/mm-wave plasma diagnostics.